Adaptive and compliant wingtip devices enabled by additive manufacturing and multistable structures

Kimberly Gustafson^a, Luis Urrutia^a, Alexander Pankonien^b, Gregory Reich^b, Aimy Wissa^a

^aUniversity of Illinois at Urbana-Champaign, 105 South Matthews Ave., Urbana, IL, USA 61801; ^bU.S. Air Force Research Laboratory, Wright–Patterson Air Force Base, Ohio 45433

ABSTRACT

Multifunctional lifting surfaces can expand the mission capabilities of aerial vehicles with a minimal number of components added to the vehicle. This paper presents a bio-inspired segmented wingtip concept for lift enhancement enabled by passive structural tailoring and active bistable truss mechanisms. The development of wingtips stems from studies of birds with desirable flight capabilities. The structural characteristics and maneuverable changes of a bird's primary feathers during flight have identified three notable feather degrees of freedom: **incidence angle**, **dihedral angle**, and gap spacing. Wind tunnel experiments conducted on multi-wingtip systems have determined that different wingtip orientations and spacings are desired to enhance aerodynamic performance depending on the flight conditions. These results suggest that the wingtip degrees of freedom must be varied during flight to achieve optimal aerodynamic performance. This paper presents two structural concepts, one passive and one active, to achieve desired morphological wingtip parameters during flight. The passive structural concept exploits bend-twist coupling of additively manufactured composite laminate wingtips by using aerodynamic loads to induce passive shape adaptation of the composite wingtips to control the twist and dihedral angles. The active concept utilizes bistable truss mechanisms to vary the wingtip gap spacing. The force-displacement responses of bistable mechanisms and the bending and twist of bend-twist coupled composite wingtips are measured using a universal testing machine and Digital Image Correlation, respectively. Experimental results include the energy storage characterization of the bistable mechanisms as a function of material characteristics and the bend-twist coupling of the composite wingtips as a function of fabrication process and laminate properties.

Keywords: Incidence angle – wingtip angle of attack relative to the base wing angle of attack, dihedral angle – angle between the span of the base wing and the span of a wingtip, gap spacing – chordwise distance between wingtips expressed as a percent of the base wing chord length

1. INTRODUCTION

The shape morphing wing technology outlined by Sofla et. al.¹ and Barbarino et. al.² focused on the ability to control the span, chord, and camber of a wing. However, the design and motion control of a multi-wingtip system for aerodynamic enhancement has not been studied extensively^{3,4,5}. Changing the shape and orientation of wingtips has both mechanical and efficiency advantages over adjusting the entire wing⁶. A morphing multi-wingtip system enables the actuation and adaptability of independent wingtips for flight condition requirements and enhanced aircraft performance.

Whitcomb⁷ was one of the first to conduct wingtip experiments by comparing the performance of a wing with a winglet to a wing with a planar wing extension. Whitcomb's results showed that the winglet doubled the lift-to-drag ratio (L/D) of the wing and reduced induced drag by up to 20%. This reported reduction in induced drag can increase the cruising range of an aircraft by as much as 7%. More recent interest in wingtips has stemmed from studies done to characterize bird wings both during flight and in wind tunnel experiments^{8,9,10}. To provide context of the contribution of this work compared to other work in the literature, we have identified the three wingtip degrees of freedom shown in Figure 1 inspired by the mobility of birds' primary feathers that adapt to changing flight conditions.



Figure 1. Primary feather degrees of freedom adapted during flight: (a) incidence angle (b) dihedral angle (c) gap spacing.

Tucker¹¹ conducted wind tunnel experiments on Harris Hawk wings to determine the effect of segmented wingtips by comparing hawk wings with tip feathers to hawk wings with clipped tip feathers. The results showed that the tip feathers induced only 70-90% of the drag induced by clipping the tip feathers, meaning that wingtips favorably reduce induced drag. Hoey¹² investigated the impact of wingtip feathers on static stability during soaring for large birds such as ravens and seagulls. This study concluded that soaring stability is sensitive to the dihedral angle of the wingtip feathers. These studies have provided evidence that wingtip feathers improve the aerodynamic efficiency of bird wings, and therefore, promote the development of an adaptive multi-wingtip design for aircraft.

Many engineered multi-wingtip designs have been evaluated to demonstrate their advanced performance potential over a baseline wing or an equivalent single winglet^{3,4,5}. Miklosovic³ noted that high dihedral angles are detrimental to lift due to the loss of effective planform area and recommended that multiple wingtips be kept at dihedral angles less than 45 degrees for enhanced lift. This study also observed that the leading wingtip has the most pronounced effect on increasing lift, and that certain dihedral configurations increased the lift coefficient by as much as 65%. Lynch et. al.⁴ studied the effects of varying the gap spacing between wingtips for a three-wingtip system. This experiment showed that a wingtip gap spacing of 20% of the base wing chord showed a 5.6% improvement in the maximum coefficient of lift compared to wingtips with zero spacing. The incidence angle of wingtips was studied by Lynch et. al.⁴ and Smith et. al.⁵, with both showing similar results that a leading edge wingtip with a negative incidence produced a higher coefficient of lift at pre-stall angles of attack when compared to a configuration with zero incidence. Spillman et. al.¹³ similarly concluded that negative incidence wingtips improved L/D by up to 25%. These observations have suggested that a multi-wingtip device capable of varying dihedral, incidence, and gap spacing will exhibit improved aerodynamic performance under changing flight conditions. While the aforementioned studies have considered one or two of the bioinspired degrees of freedom, very little work has been done to consider the aerodynamic effect of all three, and no studies have considered a structural design to implement these degrees of freedom on an engineered wing.

This paper describes a novel morphing concept inspired by the dihedral angle, incidence angle, and gap spacing of bird feathers. Figure 2 shows an adaptable multi-wingtip system concept, where the wingtip gap spacing is controlled actively using bistable mechanisms, and the dihedral and incidence angles of each wingtip are controlled passively through composite bend-twist coupling. The paper begins with an overview of bend-twist coupled composite materials and bistable mechanisms in Sections 2.1 and 2.2, respectively. Section 3.0 details the experimental setup and fabrication techniques. The results section, Section 4, shows the feasibility of using the concept shown in Figure 2 to achieve the desired degrees of freedom to improve aerodynamic performance. Concluding remarks include a comparison of experimental results with the desired bending (dihedral), twisting (incidence) and gap spacing (actuator stroke) parameters found in literature for multi-winglet systems.

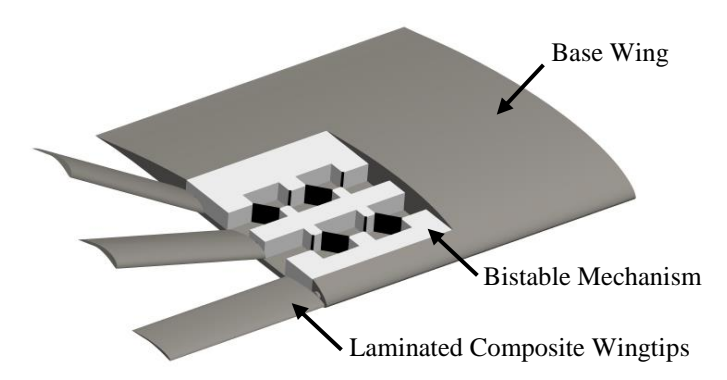


Figure 2. Conceptual design of an adaptive multi-wingtip system that utilizes bend-twist coupled composite wingtips to passively control wingtip incidence and dihedral angles and a bistable mechanism to actively control wingtip gap spacing.

2. TECHNICAL APPROACH

2.1 Technical background – bend-twist coupling in composites

For the adaptive wingtip concept shown in Figure 2, a moment induced on a wingtip by the lift forces during flight will cause a bending deflection (i.e. a change in dihedral angle). Through exploiting the bend-twist coupling composite properties in each wingtip, this bending deflection will induce twist, effectively changing the wingtip incidence angle. Thus, the bend-twist shape adaptation of the composite wingtips will vary by the amount of aerodynamic load experienced by the wingtip, allowing for passive control of the wingtip dihedral and twist angles. The focus of this work is to exploit the bend-twist coupling of composites, which is a function of the stacking sequence of the laminate and fiber orientation of each lamina (single layer of a laminate).

The mechanical properties of a laminate have been well described using the Classical Laminated Plate Theory. ¹⁴ A laminate is constructed by stacking N laminas in the z direction (thickness). The x-y axes used to define the strains and curvatures in the laminate are located at the geometric midplane in the z direction, where ε_{xx}^0 , ε_{yy}^0 and γ_{xy}^0 are the normal and midplane shear strains, and k_{xx} , k_{yy} , and k_{xy} are the bending and twisting curvatures of the laminate, respectively. The constitutive equations, obtained by integrating the stresses over the thickness of the laminate, relate the applied forces and moments to the strains and curvatures in the laminate. The constitutive equations of a symmetric laminate are of the form

and

$$\begin{pmatrix} M_{xx} \\ M_{yy} \\ M_{xy} \end{pmatrix} = \begin{bmatrix} D_{11} & D_{12} & D_{16} \\ D_{12} & D_{22} & D_{26} \\ D_{16} & D_{26} & D_{66} \end{bmatrix} \begin{pmatrix} k_{xx} \\ k_{yy} \\ k_{xy} \end{pmatrix},$$
 (2)

where N_{xx} , N_{yy} , and N_{xy} are the in-plane normal and shear forces per unit width, and M_{xx} , M_{yy} , and M_{xy} are the bending and twisting moments per unit width, respectively. [A] and [D] are the extensional and bending stiffness matrices of the laminate with units N/m and N*m, respectively. These stiffness matrices are functions of the general orthotropic lamina stiffness matrix, \bar{Q}_j , given by

$$A_{mn} = \sum_{j=1}^{N} (\bar{Q}_j)(h_j - h_{j-1})$$
(3)

and

$$D_{mn} = \frac{1}{3} \sum_{j=1}^{N} (\bar{Q}_j) (h_j^3 - h_{j-1}^3)$$
(4)

for the j^{th} lamina whose top and bottom surfaces are at distances (h_{j-1}) and (h_j) from the midplane of the laminate, respectively. Equation 2 shows that bending and twisting moments induce only curvature changes and not in-plane strains. For a laminate exposed to lift forces during flight, the applied moments M_{yy} and M_{xy} are absent, reducing Equation 2 to

$$k_{xx} = d_{11}M_{xx}$$

 $k_{yy} = d_{12}M_{xx}$
 $k_{xy} = d_{16}M_{xx}$, (5)

where the matrix [d] is the inverse of the bending stiffness matrix [D]. The bend-twist coupling parameter d_{16} relates the laminate bending to the resulting laminate twist. This bend-twist coupling parameter may therefore be engineered to achieve a desired laminate twist angle given a specified bending moment (from applied lift forces) by tuning the fiber orientation angle of each lamina and the stacking sequence of the laminate.

2.2 Technical background – bistable structures

While the twist and dihedral angles of the wingtips are passively controlled using bend-twist coupling, the desired spacing between the wingtips will be actively achieved by combining smart actuators with bistable mechanisms. The bistable mechanism allows for the efficient use of smart actuators by reducing the power required to change and maintain the spacing between the wingtips. Figure 3 is a representative force-displacement curve and corresponding energy-displacement profile for a bistable mechanism. The displacements where the force is zero and the energy is at a local minimum represent the stable equilibrium positions of the mechanism. The central location on the curve where the force is equal to zero is an unstable equilibrium passed through during the transition of the mechanism between the stable positions. The area under the positive region of the force-displacement curve represents the input energy required to transition the mechanism from the first stable equilibrium position to the second. The energy under the negative region of the force-displacement curve (the output energy) is the energy required to return the structure to the initial stable position. The output energy is a metric used to quantify the bistability of the mechanism. As the output energy increases, the level of bistability in the mechanism also increases. The difference between the input and output energy values is the amount of strain energy stored in the mechanism.

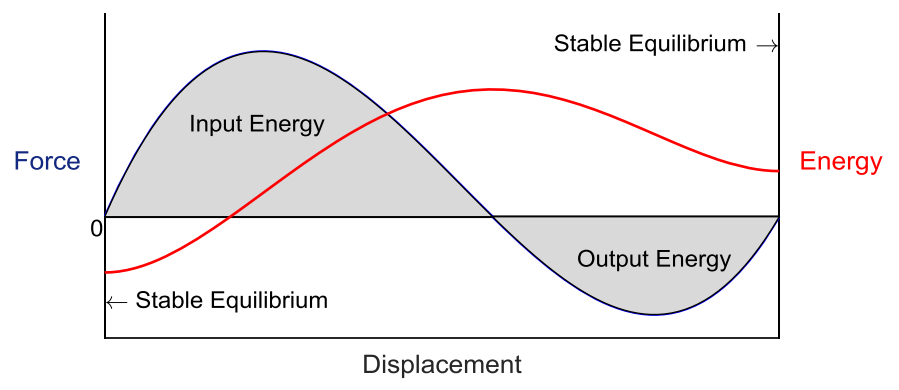


Figure 3. Representative bistable force-displacement curve and corresponding energy-displacement profile. The locations where the force is zero and the energy is a local minimum represent the stable equilibrium positions of the mechanism. The difference between the input and output energy values is the strain energy stored in the mechanism, and the output energy is proportional to the bistability of the mechanism.

Multiple bistable structures have been proposed as linear actuation mechanisms. Figure 4 shows two examples of such structural arrays. Structure (a) was proposed by Pontecorvo et. al. 15 as a method of deploying a wing slat, and structure (b) has been proposed by Shan et. al. 16 as a scalable bistable mechanism that can be geometrically tuned to achieve desired input and output energy values.

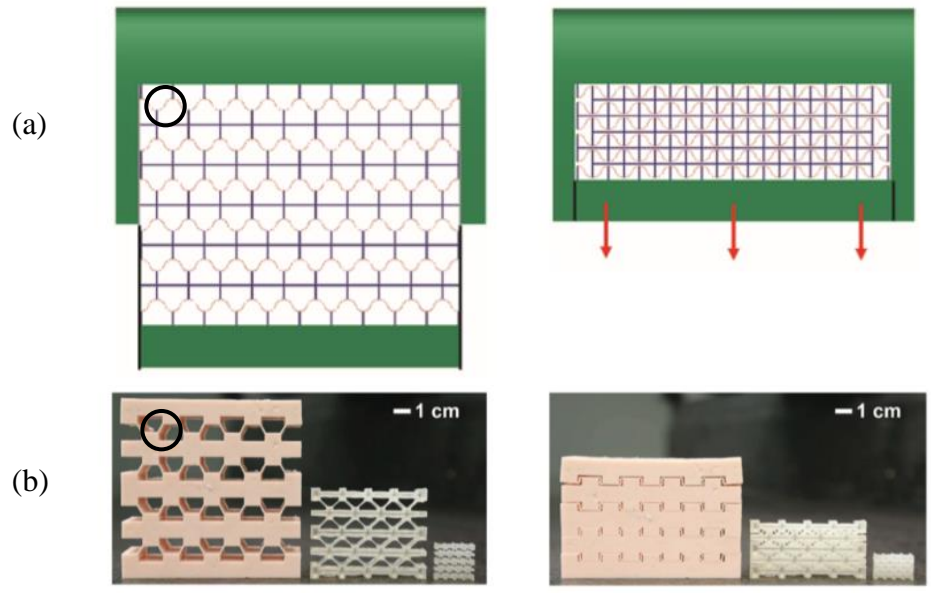


Figure 4. Bistable structures used as linear actuation mechanisms shown in both stable configurations (expanded and collapsed). (a) Structural array designed by Pontecorvo et. al. 15 as a method of deploying a wing slat. (b) Geometrically tunable mechanism designed by Shan et. al. 16 to achieve target input and output energy values.

Both structures utilize bistable beam buckling with slightly different boundary conditions. A single repeating beam element of each structure is circled. The study conducted by Shan et. al. 16 determined that the geometry of the repeating bistable element affects the bistability and energy storage capabilities of the structure. This paper investigates the same beam element considered by Shan et. al. 16, but explores the effects of changing the compliance of the bistable element and its boundary conditions by varying material composition, rather than geometry. This new approach increases the mechanism design space and allows for bistable designs that may not be possible by varying only the geometry.

3. EXPERIMENTAL METHODS

3.1 Fabrication method and test specimen details

The composite wingtips and bistable mechanisms were 3D printed using a Stratasys Objet printer and materials VeroWhite Plus and TangoBlack Plus. The TangoBlack and VeroWhite elastic moduli have been experimentally established by Pankonien et. al.¹⁷, and their respective Poisson's ratio values were taken from testing conducted by Li et. al.¹⁸.

The composite wingtips were printed using TangoBlack as the matrix material and VeroWhite as the fiber material, with a fiber volume fraction of 0.6. The TangoBlack and VeroWhite composite material properties were calculated using the law of mixtures. Table 1 is a summary of the material properties of the composite wingtip.

Table 1. Material properties of a composite made from TangoBlack and VeroWhite calculated using the law of mixtures

E ₁ (MPa)	$E_2 = E_3 (MPa)$	$v_{12} = v_{13}$	V23	$G_{12} = G_{13} \text{ (MPa)}$	G ₂₃ (MPa)
1800	2.50	0.394	0.155	0.839	0.757

For this initial investigation into bend-twist coupling, the composite wingtips were modeled as composite beams. The dimensions of the composite wingtip were defined similarly to the wingtip designed by Lynch et. al.⁴, with a length, width and thickness of 90 mm, 25 mm, and 4 mm respectively. The wingtip composite laminate was composed of eight laminas, each with a thickness of 0.5 mm. Each lamina contained fibers oriented at a certain angle with respect to the wingtip x-axis shown in Figure 5a. The orientation of the laminate was determined by calculating and maximizing the d₁₆ term similar to the approach detailed by Santiuste et. al..¹⁹

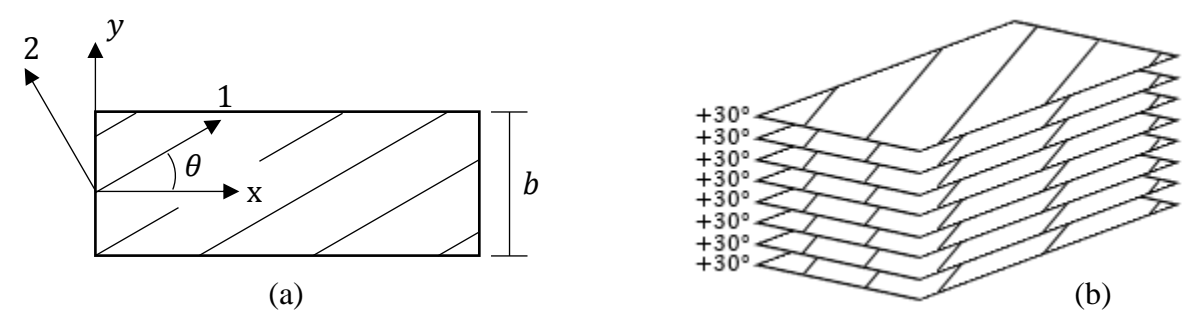


Figure 5. (a) Definition of the principal material axes (1-2) and loading axes (x-y) of a lamina, where the angle between the x axis and the 1-axis is the fiber orientation angle θ (b) The symmetric composite stacking sequence [30]₈ used to investigate bend-twist coupling as a means of passively controlling wingtip dihedral and twist angles.

Figure 6 shows the bend-twist coupling amplitude d_{16} for the stacking sequence of an 8-ply laminate $[\theta]_8$ for all fiber orientation angles. The maximum bend-twist coupling occurs in laminate $[27]_8$, with a d_{16} value of -65.6(Nm)⁻¹. However, for fabrication purposes, in this study a laminate stacking sequence of $[30]_8$ was selected, shown in Figure 5b, with a d_{16} of -64.6(Nm)⁻¹. This stacking sequence was used to construct a composite wingtip to analyze the coupling behavior of the wingtip under a given applied moment.

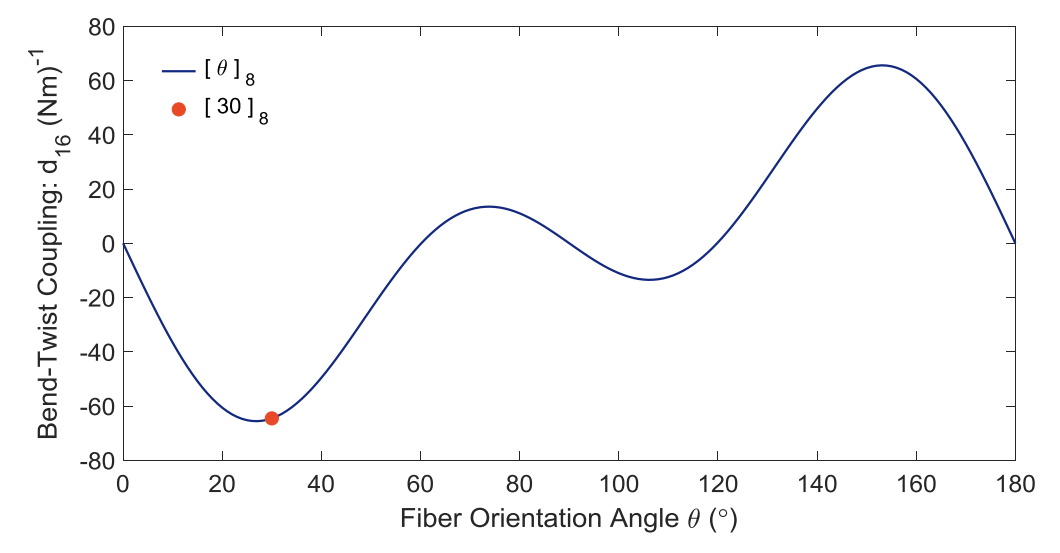


Figure 6. Bend–twist coupling amplitude versus fiber orientation angle for the 8-ply laminate stacking sequence [0]8. The stacking sequence [30]8 was selected to investigate bend-twist coupling as a means of passively controlling wingtip dihedral and twist angles.

Bistable truss mechanisms were manufactured using the beam element parameters shown in Figure 7a. The beam geometry was chosen to match the values tested in Shan et. al. 16 to provide a baseline comparison, with a length (L) of 11.2mm, a thickness to length ratio (t/L) of 0.12, and a beam angle (θ) of 40°. This beam geometry was found to be bistable by Shan et. al. 16 for a uniform beam material. In this experiment, the geometry of the beams has been kept constant to observe the effects of varying the material properties of the beam. In addition to varying the compliance of the beam, the material composition of the joints on either end of the beam (Joint 1 and Joint 2) were varied to determine the effects of compliant boundary conditions on the bistability of the truss mechanism (Figure 7b).

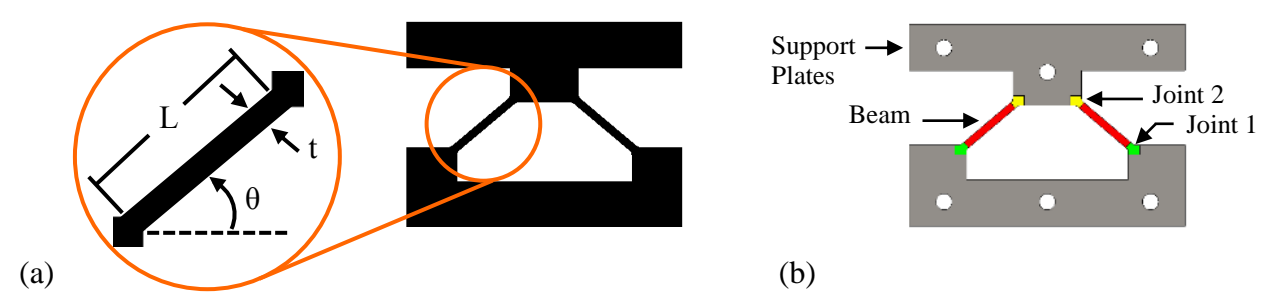
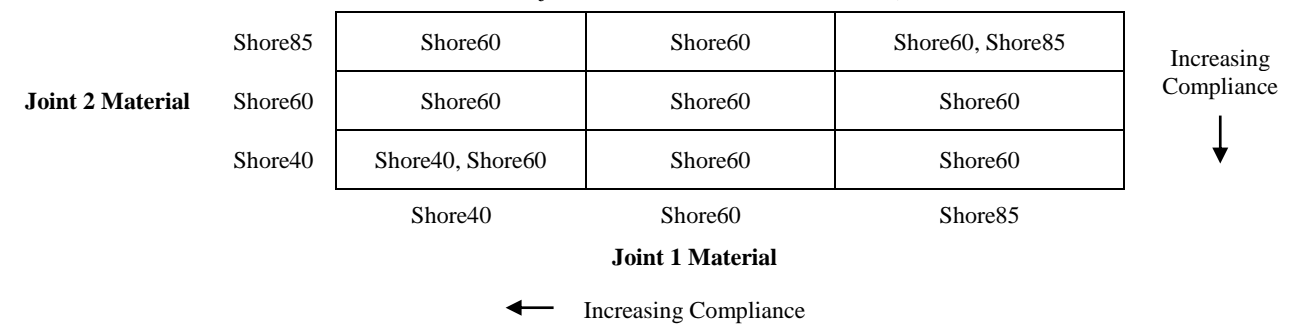


Figure 7. (a) Schematic of a single truss mechanism including two bistable beam elements. The geometric parameters of a single beam are shown, where L represents the beam length, θ the beam orientation, and t/L the relative beam thickness (b) Model of a manufactured truss mechanism showing the joint and beam geometries.

The truss mechanisms were 3D printed from the Stratasys Objet materials Shore40, Shore60, and Shore85, obtained by mixing various percentages of VeroWhite Plus and TangoBlack Plus, with a higher numerical identifier representing a less compliant material (i.e. Shore40 is more compliant than Shore60). Each truss mechanism contained two bistable beam elements supported by rigid VeroWhite Plus support plates to ensure that all deformation and energy storage occurred in the bistable elements. Table 2 is the experimental test matrix of the joint and beam material composition of each truss.

Table 2. Test matrix of beam material and corresponding joint materials for each truss mechanism, where a higher numerical identifier represents a less compliant material. (i.e. the truss mechanism represented by the top left cell has beam material Shore60 and joint materials Shore40 and Shore 85).



3.2 Experimental setup for composite wingtip beams and bistable truss mechanisms

To characterize the bend-twist coupling of a composite laminate wingtip, a point load was applied at the free end of a clamped-free composite wingtip, as shown in Figure 8, by hanging discreet mass values ranging from 50g to 400g. A two-camera stereovision system (3D DIC) was used to capture the resulting deflection of the wingtip in the z direction.

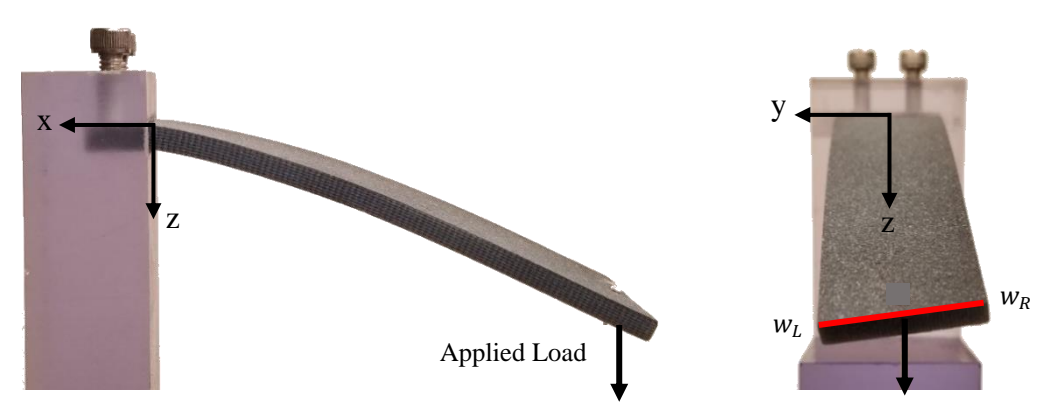


Figure 8. Experimental setup for discrete bend-twist characterization of composite wingtips with clamped-free boundary conditions and applied point load. The red line indicates the location of the applied load and measured deflection and twist. w_R and w_L are the deflections in the z direction at the right and left edges of the free end of the wingtip, respectively.

The maximum bending deflection and twist were measured along the red line shown in Figure 8. The bending deflection and the wingtip twist were calculated using Equations 6 and 7, respectively,

$$w = \frac{|w_R - w_L|}{2} \tag{6}$$

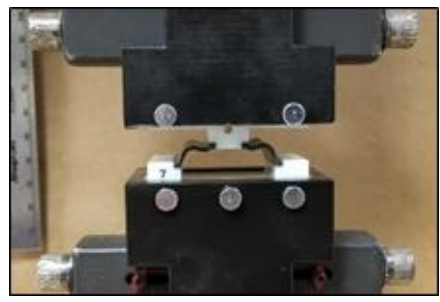
and

$$\theta_x = \sin^{-1}\left(\frac{w_R - w_L}{h}\right),\tag{7}$$

where θ_x was the twist angle about the x-axis at the free end of the wingtip, w_R and w_L were the vertical displacements of the left and right edges of the wingtip where the load was applied, respectively, and b was the wingtip width (Figure 5a).

The force-displacement response of the bistable truss mechanisms was used to determine how the material properties of the bistable beam element affect the bistability of the mechanism. A universal force testing machine was used to record the force-displacement behavior of all truss material combinations in compression. The top and bottom support plates were pinned to the jaws of the force machine to ensure the ability to record negative force values as snap through occurred between the two stable positions of the mechanisms. Figure 9 shows the progression of a truss mechanism as it was compressed by the universal testing machine.





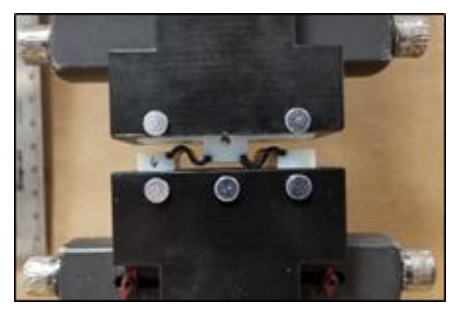


Figure 9. Progression of a bistable truss mechanism being compressed by a universal testing machine. The rigid top and bottom support plates of the truss were pinned to the jaws of the testing machine to ensure the ability to record negative force values and localize all deformation and energy storage in the bistable elements.

4. RESULTS

4.1 Characterization of the displacement and twist of a bend-twist coupled composite wingtip

The bend-twist coupling response of the composite wingtip was quantified by measuring the bending displacement and twist at the free end of the cantilevered wingtip. The bending displacement was transformed to dihedral angle using an estimated geometrical relation between the wingtip length and bending displacement for comparison with desired dihedral parameters found in literature for multi-winglet systems. Figure 10 shows the dihedral and twist response of the composite wingtip layup [30]₈ for applied loads ranging from 50g to 400g.

For maximized lift, Lynch et. al. 4 determined that a three-wingtip system should have twist angles of -10° , -5° , and 0° for the leading, middle, and trailing edge wingtips, respectively. Moreover, at a Reynold's number of 100,000, Lynch et. al. observed lift forces between 3.0N and 4.6N. For an applied load of 400g ($\sim3.9N$), the [30] $_8$ composite wingtip achieved a twist angle of -8.3° . This result has shown the feasibility of designing a composite wingtip to passively achieve twist angles up to the desired value of -10° .

Miklosovic³ tested a three-wingtip system with various combinations of wingtip dihedral angles including $20^{\circ}/10^{\circ}/0^{\circ}$, $40^{\circ}/20^{\circ}/0^{\circ}$, and $60^{\circ}/30^{\circ}/0^{\circ}$ defined from leading edge to trailing edge respectively. These configurations produced 7-12% higher lift when compared to a configuration of $0^{\circ}/0^{\circ}/0^{\circ}$. The [30]₈ composite wingtip tested in this study achieved dihedral angles between 5.1° and 38.2° . These tested values achieved nearly the entire range of dihedral angles required to achieve the high-lift configurations found by Miklosovic³.

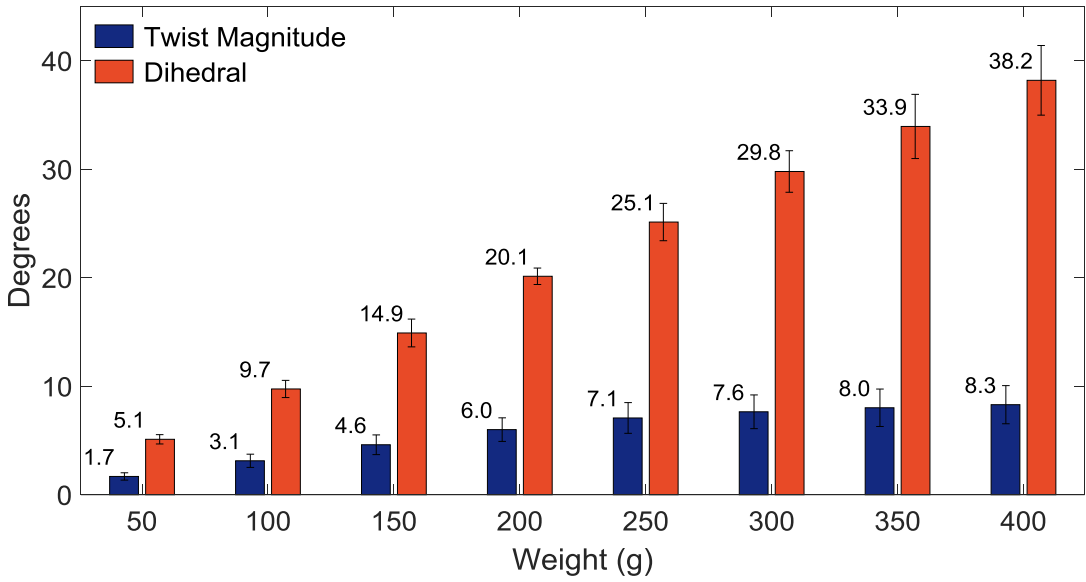


Figure 10. Bend-twist coupled response of the [30]₈ wingtip composite layup for discrete applied loads ranging from 50g to 400g.

Based on the results by Lynch et. al.⁴ and Miklosovic.³, the optimum wingtip parameters for a multi-wingtip system depend on the desired performance specifications (i.e. maximizing lift vs. maximizing L/D ratio). For a given lift force and resulting dihedral angle, the amount of wingtip twist can be controlled by adjusting the composite laminate sequence and fiber orientation as indicated in Figure 6. This allows each of the wingtips to have different twist and dihedral angles under a given load (lift). Under applied loads up to 3.9N, the [30]₈ composite wingtip achieved a maximum dihedral angle of 38.2° and corresponding twist angle of -8.3°. These results have demonstrated the feasibility of using a composite wingtip to achieve the desired bending and twist values required for improved aerodynamic performance.

4.2 Characterization of bistable truss mechanisms

The force-displacement response of each truss mechanism was recorded to observe how the compliance of the bistable element affected the actuation force and bistability of the mechanism. Figure 11a is the force-displacement behavior of the trusses whose bistable elements were printed from a single uniform material.

As the compliance of the bistable element decreased (from Shore40 to Shore85), the force required to transition the truss mechanism between the first and second stable positions increased along with the strain energy in the mechanism. However, the force required to return to the initial position decreased, making the mechanism less bistable. For the truss with bistable element material Shore85, the applied force was always greater than zero, meaning the mechanism never reached a bistable equilibrium. These results demonstrated that for a given truss geometry, varying the compliance of the bistable element expanded the design space of the mechanism actuation force and bistability. To further expand the mechanism design space, the bistable element was divided into the central bistable beam component and boundary conditions shown in Figure 7b. The bistable beam material was held constant at the intermediately compliant material (Shore60), and the compliance of the joints on either end of the beam were varied according to the test matrix in Table 2. The resulting force-displacement responses are shown in Figure 11b.

Figure 11b shows that, for a fixed beam compliance, more compliant boundary conditions resulted in a lower actuation force and higher required force to return to the initial configuration. Alternatively, less compliant boundary conditions resulted in higher actuation forces and a truss combination that did not exhibit bistability (the case where both joints were less compliant than the beam element). To obtain a better understanding of the bistability of the mechanisms, the input and output energy values for the mechanisms were calculated from the area under the force-displacement curves and are shown in Figure 12a and 12b respectively. As mentioned previously, the output energy required to return the truss mechanism to the original configuration is proportional to the bistability of the mechanism. Figure 12c shows the output energy of each truss mechanism normalized with respect to the required input energy of the mechanism, which is a metric of the bistability of the mechanism. As the compliance of the joints increased, the input energy required to transition the mechanism between

stable positions decreased, and the bistability of the mechanism increased. Furthermore, the truss mechanism with both joints less compliant than the beam element did not exhibit any bistability (i.e. force always greater than zero).

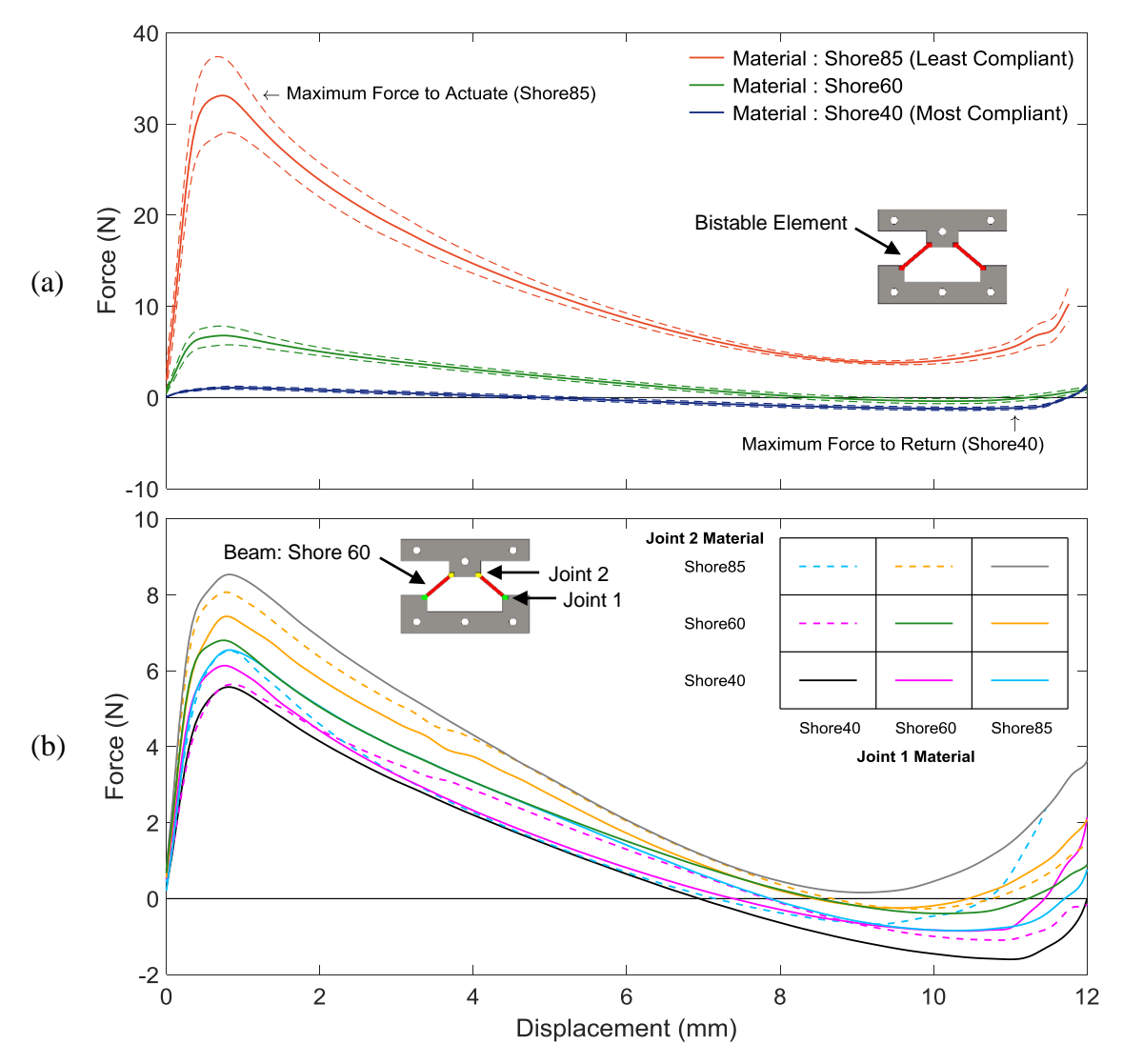


Figure 11. (a) Force-displacement characterization of truss mechanisms with bistable elements printed from a single uniform material, where a more compliant bistable element resulted in a decreased actuation force and increased return force. (b) Force-displacement characterization of truss mechanisms with bistable beam material Shore60 and variable joint compliance on either end of the beam, ranging from Shore40 (most compliant) to Shore85 (least compliant).

Figure 11a showed that, for a given geometry, varying the compliance of the bistable element of the truss mechanism varied the required actuation force and bistability of the mechanism. In addition, Figures 11b and 12 showed that adjusting the compliance of the boundary conditions of the bistable element allowed for even finer tuning of the mechanism actuation force and bistability.

To use a bistable truss mechanism as a means of actuating the wingtip gap spacing, the truss needs to be tuned and scaled for the desired actuation force and gap spacing. The truss geometry for the tests conducted in this study was chosen to replicate the geometry data from Shan et. al. 16 to give a baseline comparison. However, the length of the bistable element (L), identified in Figure 7a, can be scaled to achieve the desired actuation stroke while maintaining the bistability of the structure by keeping the same beam angle (θ) and thickness to length ratio (t/L). In addition, the results have shown that the force required to actuate the truss mechanism (increase and decrease the wingtip spacing) can be tuned through the material composition of the beam and joints that make up the bistable element of the truss mechanism.

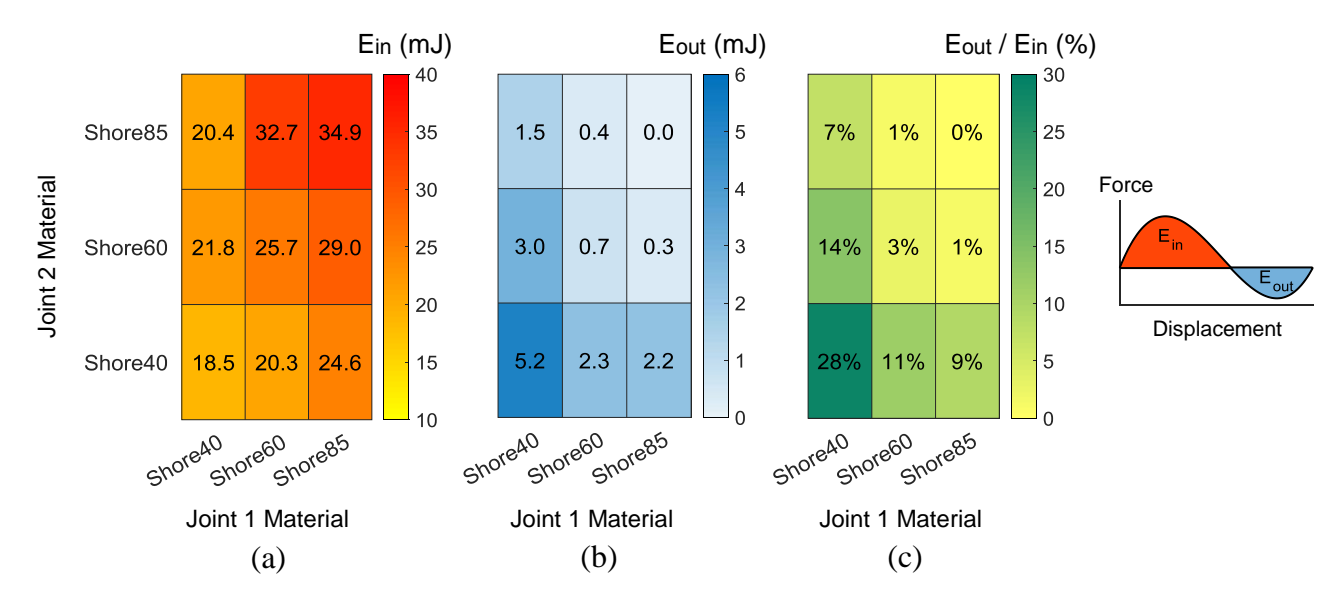


Figure 12. (a) Input energy required to compress the truss mechanisms between stable positions for beam material Shore60 and variable joint compliance ranging from Shore40 to Shore85. (b) Output energy required to return the truss mechanisms to the initial stable position, which is proportional to the bistability of the mechanism. (c) Bistability metric expressed as the output energy normalized with respect to the input energy.

5. CONCLUSION

This paper presented a bio-inspired segmented wingtip concept for lift enhancement enabled by passive structural tailoring and active bistable truss mechanisms to control the dihedral angle, twist angle and gap spacing of individual wingtips. A bend-twist coupled composite wingtip was used to passively control the dihedral and twist angles. Results showed that the feasible range of wingtip dihedral and twist angles achieved by composite coupling were within the desired range for lift enhancement. However, a model is required to design and optimize the laminate stacking sequence and material properties for ideal aerodynamic performance. Moreover, a bistable mechanism was proposed to actively control the wingtip gap spacing while minimizing the energy required to vary and maintain the wingtip spacing. Results showed that, in addition to geometry, material properties and boundary conditions can be used to tailor the mechanism's level of bistability and required actuation force, enabling the use of a wide range of actuators.

Future work includes tailoring the bistable mechanism and composite wingtips to meet wing-sizing requirements and aerodynamic criteria. Actuator selection and wind tunnel testing will be performed to characterize the aerodynamic performance of the adaptive multi-wingtip system in flight-like conditions for symmetric and asymmetric wingtip actuation.

ACKNOWLEDGEMENTS

This work was funded as part of the Wright Patterson Air Force Research Laboratory Summer Faculty Fellowship Program. Resources from the SLOAN foundation and the University of Illinois at Urbana-Champaign Mechanical Science and Engineering department and Material Testing Laboratory are also appreciated.

REFERENCES

- [1] Sofla, A.Y.N., Meguid, S.A., Tan, K.T. and Yeo, W.K., "Shape Morphing of Aircraft Wing: Status and Challenges," Materials and Design, 31 (3), 1284-1292 (2010).
- [2] Barbarino, S., Bilgen, O., Ajaj, R. M., Friswell, M. I. and Inman, D. J., "A review of morphing aircraft," J. Intell. Mater. Syst. Struct., 22(9), 823–77 (2011).
- [3] Miklosovic, D., "Analytic and experimental investigation of dihedral configurations of three-winglet planforms," J. Fluids Eng., 130 (7), 0711103/1–0711103/10 (2008).
- [4] Lynch, M., Mandadzhiev, B., and Wissa, A., "Bioinspired wingtip devices: A pathway to improve aerodynamic perfromance during low Reynolds number flight," J. Bioinspiration Biomimetics, 13(3), (2018).
- [5] Smith, M., Komerath, N., Ames, R., Wong, O., Pearson, J., "Performance analysis of a wing with multiple winglets," AIAA Paper-2001-2407, (2001).
- [6] Falcão, L., Gomes, A. and Suleman, A., "Design and Analysis of an Adaptive Wingtip," ASC Structures, Structural Dynamics and Materials Conference, (2011).
- [7] Whitcomb, R., "A Design Approach and Selected Wind-Tunnel Results at High Subsonic Speeds for Wing-Tip Mounted Winglets," NASA TN D8260, (1976).
- [8] Graham, R.R., "Safety devices in wings of birds," Journal Royal Aerospace Society, 36 (253), 24-58 (1932).
- [9] Pennycuick, C., Obrecht, H. H., & Fuller, M. R.," Empirical estimates of body drag of large waterfowl and raptors," Journal of Experimental Biology, 135(1), 253-264 (1988).
- [10] Withers, P. C., "An aerodynamic analysis of bird wings as fixed aerofoils," Journal of Experimental Biology, 90(1), 143-162 (1981).
- [11] Tucker, V.A., "Drag reduction by wing tip slots in a gliding harris' hawk, parabuteo unicinctus," J. Exp. Biol. 198 (3) 775–81 (1995).
- [12] Hoey, R. G., "Research on the stability and control of soaring birds," Proc. 6th AIAA, 393-402 (1992).
- [13] Spillman, J.J., "The use of wing tip sails to reduce vortex drag," Aeronautical Journal, 387-395 (1977).
- [14] Mallick, P. K., [Fiber-Reinforced Composites], Marcel Dekker, New York, (1993).
- [15] Pontecorvo, M., Barbarino, S., Murray, G., Gandhi, F., "Bistable Arches for Morphing Applications," Journal of intelligent Material Systems and Structures, 24(3), 274-286 (2012).
- [16] Shan, S., Kang, S. H., Raney, J. R., Wang, P., Fang, L., Candido, F., Lewis, J. A. and Bertoldi, K. (2015)," Multistable Architected Materials for Trapping Elastic Strain Energy," Adv. Mater., 27 (29), 4296-4301 (2015).
- [17] Pankonien, A., and Reich, G.W., "Multi-Material Printed Wind Tunnel Flutter Model," AIAA Journal, 56(2), 1-15 (2017).
- [18] D. Li, L. Dong and R. S. Lakes, "A unit cell structure with tunable Poisson's ratio from positive to negative", Mater. Lett., 164, 456–459 (2016).
- [19] Santiuste, C., Sanchez-Saez, S., Barbero, E., "Dynamic analysis of bending-torsion coupled composite beams using the flexibility influence function method," Int J Mech Sci, 50 (12), 1611-1618 (2018).

Proc. of SPIE Vol. 10965 109650J-12